

Fully Hyperbolic Neural Networks: A Novel Approach to Studying Aging Trajectories

Hugo Ramirez, Davide Tabarelli^{ID}, Arianna Brancaccio^{ID}, Paolo Belardinelli^{ID}, Elisabeth B. Marsh, Michael Funke, John C. Mosher^{ID}, Fernando Maestú^{ID}, Mengjia Xu^{ID}, Member, IEEE, and Dimitrios Pantazis^{ID}

Abstract—Characterizing age-related alterations in brain networks is crucial for understanding aging trajectories and identifying deviations indicative of neurodegenerative disorders, such as Alzheimer’s disease. In this study, we developed a Fully Hyperbolic Neural Network (FHNN) to embed functional brain connectivity graphs derived from magnetoencephalography (MEG) data into low dimensions on a Lorentz model of hyperbolic space. Using this model, we computed hyperbolic embeddings of the MEG brain networks of 587 individuals from the Cambridge Centre for Ageing and Neuroscience (Cam-CAN) dataset. Notably, we leveraged a unique metric—the radius of the node embeddings—which effectively captures the hierarchical organization of the brain, to characterize subtle hierarchical organizational changes in various brain subnetworks attributed to the aging process. Our findings revealed that a considerable number of subnetworks exhibited a reduction in hierarchy during aging, with some showing gradual changes and others undergoing rapid transformations in the elderly. Moreover, we demonstrated that hyperbolic features outperform traditional graph-theoretic measures in capturing age-related information in brain networks. Overall, our study represents the first evaluation of hyperbolic embeddings in MEG brain networks for studying aging trajectories, shedding light on critical regions undergoing

significant age-related alterations in the large cohort of the Cam-CAN dataset.

Index Terms—Aging trajectories, Alzheimer’s disease, age prediction, magnetoencephalography, brain networks, hyperbolic space, graph embedding.

I. INTRODUCTION

ALZHEIMER’S disease (AD) is a global public health priority, particularly affecting older populations. Characterized by a gradual and relentless neurodegenerative process, AD includes a prolonged asymptomatic preclinical phase before the onset of mild cognitive impairment and significant cognitive decline. Remarkably, the complex brain processes, including amyloid deposition, tau phosphorylation, and neuroimaging changes, that lead to AD can begin more than two decades before clinical symptoms appear [1]. These early changes provide valuable opportunities to monitor shifts in brain health that may precede the onset of symptoms or the disease itself. Observations of these changes can be combined with established risk factors, such as age.

Recent breakthroughs in AD treatments have shown the greatest benefits in early-stage patients [2], making it crucial to assess early deviations from typical *aging trajectories* [3]. Early intervention could slow AD progression, offering hope for improved outcomes for those eventually affected by the disease. An excellent tool for establishing normal brain aging trajectories and identifying deviations is magnetoencephalography (MEG) [4], [5]. MEG offers exceptional temporal resolution, allowing for the characterization of subtle brain changes, especially in the frequency domain [6]. Additionally, MEG captures the fields produced by intraneuronal currents, providing a more direct index of neuronal activity than biomarkers measuring hemodynamic responses, such as fMRI or FDG-PET. With MEG, researchers can generate functional connectivity maps and study distinctive patterns of alterations in functional connectivity within large-scale brain systems [4].

Despite the complex relational structure of brain connectivity networks (or graphs), most existing MEG-based neuroimaging studies rely heavily on statistical analyses using traditional graph-theoretic measures, which are based on domain knowledge but may not be optimal for capturing complex hierarchical patterns [7], [8]. Commonly used measures include node degree, closeness centrality, betweenness centrality, global

Received 4 October 2024; revised 2 December 2024 and 9 January 2025; accepted 4 February 2025. Date of publication 6 March 2025; date of current version 6 June 2025. This work was supported in part by Jameel Clinic at MIT grant award (to DP), in part by the National Institute on Aging of the National Institutes of Health under Grant RF1AG074204 (to MF, JCM, MF, FM, and DP) and Grant RF1AG079324 (to EBM, MF, JCM, MF, FM, and DP), and in part by DOE SEA-CROGS project (DE-SC0023191) to MX. (Corresponding authors: Dimitrios Pantazis; Mengjia Xu.)

Hugo Ramirez and Dimitrios Pantazis are with the McGovern Institute for Brain Research, Massachusetts Institute of Technology, Cambridge, MA 02139 USA (e-mail: hramir@mit.edu; pantazis@mit.edu).

Mengjia Xu is with the McGovern Institute for Brain Research, Massachusetts Institute of Technology, Cambridge, MA 02139 USA, and also with the Department of Data Science, Ying Wu College of Computing, New Jersey Institute of Technology, Newark, NJ 07102 USA (e-mail: mx6@njit.edu).

Davide Tabarelli, Arianna Brancaccio, and Paolo Belardinelli are with the Center for Mind/Brain Sciences, University of Trento, 38122 Trento, Italy.

Elisabeth B. Marsh is with the Department of Neurology, Johns Hopkins University School of Medicine, Baltimore, MD 21205 USA.

Michael Funke and John C. Mosher are with the Department of Neurology, McGovern Medical School, UTHealth Houston, Houston, TX 77030 USA.

Fernando Maestú is with the Department of Experimental Psychology, Complutense University of Madrid, 28040 Madrid, Spain.

Digital Object Identifier 10.1109/JBHI.2025.3540937

efficiency, and other measures assessed across pre-selected brain subnetworks, such as the default mode network and salience networks [19]. However, there is a pressing need for data-driven methods that can more effectively capture complex hierarchical structures while adapting to the data and *automatically* detecting features suitable for downstream tasks, such as modeling and characterizing brain aging trajectories.

Recent advancements in neural network models have highlighted their significant potential in embedding complex human brain networks into latent spaces, where nodes are represented as low-dimensional vectors [4], [5], [10]. Typically, graph representation learning employs graph convolutional neural networks to map graph nodes into points within Euclidean space. However, Euclidean geometry often falls short due to its limited representational capacity, leading to high distortion when applied to brain networks. This distortion arises because brain networks are scale-free graphs with a hierarchical, tree-like structure, where the number of nodes increases exponentially as one moves from higher to lower hierarchical levels. This exponential growth exceeds the polynomial expansion capacity of Euclidean space, resulting in distorted embeddings [11].

In contrast, hyperbolic space, characterized by its negative curvature, effectively addresses the exponential growth of nodes in scale-free brain graphs [5]. The hyperbolic geometry expands exponentially as one moves away from the center, mirroring the growth patterns of brain networks. This approach offers several advantages for embedding brain networks, such as minimal distortion and preservation of both local and global geometric information. It enables faithful embeddings even in low-dimensional spaces, which benefits downstream tasks including the characterization of age trajectories, and the development of neural network models with lower complexity, higher generalization capacity, and reduced training data requirements [12], [13], [14].

A crucial property of hyperbolic embedding is the hierarchical organization of node embeddings: higher hierarchical regions are mapped near the center, while lower hierarchical regions are mapped towards the periphery [5]. Here, we leveraged this characteristic to delineate changes in the hierarchical structure of the brain across different ages. We designed a novel hyperbolic MEG brain network embedding framework that transforms high-dimensional, complex MEG brain networks into lower-dimensional hyperbolic representations. This involved creating and validating a new hyperbolic model based on the architecture of the fully hyperbolic neural network (FHNN) [15]. Using this model, we computed hyperbolic embeddings of the MEG brain networks of 587 individuals from the Cam-CAN dataset [16]. A unique metric—the radius of the node embeddings—was employed to effectively proxy the hierarchical organization of the brain. We utilized this metric to characterize subtle changes in the hierarchical organization of various brain subnetworks attributed to the aging process.

Our findings revealed that a considerable number of subnetworks exhibit a reduction in hierarchy during aging, with some displaying slow changes and others undergoing faster changes across age. Overall, our study presents the first evaluation of hyperbolic embeddings in MEG brain networks to study aging trajectories, revealing critical regions that undergo significant

TABLE I
AGE DISTRIBUTION OF CAM-CAN SUBJECTS

Group	Age Range	Number of Subjects	Female subjects
1st Decade	18–30	67	38
2nd Decade	30–40	87	38
3rd Decade	40–50	101	53
4th Decade	50–60	85	42
5th Decade	60–70	100	47
6th Decade	70–80	92	53
7th Decade	80–90	55	24
Total Subjects	18–90	587	295

age-related alterations in the large cohort of the Cam-CAN dataset.

II. METHODS

A. Participants, Data Acquisition, and Pre-Processing

The study cohort consisted of 587 healthy participants (age range 18–89 years; 295 Female; see Table I) from the Cam-CAN dataset [16]. All subjects were tested for the absence of serious neurological and psychiatric conditions as well as the absence of cognitive decline, determined by having a Mini-Mental State Examination (MMSE) score higher than 24 [17]. The subjects were drawn from the imaging component of the Cam-CAN study, which originally included approximately 700 individuals, each undergoing different imaging protocols. For our analysis, we selected participants with complete imaging data: MEG resting-state recordings, MEG empty-room recordings (for noise covariance), and T1-weighted scans (for cortical anatomy). This initially yielded a dataset of 591 individuals, but 4 participants were excluded due to MRI segmentation errors, resulting in a final cohort of 587.

Three-minute eyes-closed resting-state MEG recordings were collected for all participants using a 306-channel VectorView MEG system (102 magnetometers, 204 first-order planar gradiometers; sampling rate = 1000 Hz; high-pass filter = 0.03 Hz; low-pass filter = 330 Hz). Pre-processing was performed using the Fieldtrip software [18] and custom MATLAB code, focusing only on the gradiometer recordings (magnetometers were excluded due to overlapping information).

During the recording, the position of the head was continuously monitored by sampling signals from the Head Position Indicator (HPI) coils. This approach enabled offline correction of head movements using the Signal Source Separation (SSS) method [19]. In addition to correcting head movements, SSS suppressed external magnetic interference and reconstructed bad channels. Data preprocessing also accounted for physiological artifacts. The data were filtered between 100 and 140 Hz, transformed to z-scores, and segments exceeding 5 standard deviations for at least 200 ms were identified as muscular artifacts and excluded. Vertical and horizontal electrooculogram (EOG) signals were recorded to track blinks and eye movements, while electrocardiogram (ECG) signals were collected using bipolar electrodes to monitor cardiac activity. An Independent Component Analysis (Infomax ICA [20]) decomposition was performed to identify components correlated with eye and

cardiac activity. These components were removed to clean the signal of these artifacts.

B. Source Reconstruction

For each participant, anatomical MRI T1-weighted images were processed to extract models of the central surface, defined as the mid-line between the gray/white matter and the pial/gray interfaces. We used a standard CAT12¹ anatomical pipeline to conduct bias normalization, denoising and skull-stripping, resulting in the central surface, the brain enclosing surface, and a high resolution surface modeling the participant head.

We then co-registered the MEG resting-state data to the subject-specific central surfaces by aligning both the anatomical landmarks and the isotrak points to the high resolution head surface. Subsequently, the central surface was decimated to the equivalent of a 5th order icosahedron, resulting in approximately 20,000 vertices with an average spatial resolution of 3.1 mm. This decimated surface served as the foundation for defining the source model for MEG source reconstruction, with dipole orientations modeled as fixed and perpendicular to the cortical mantle.

Utilizing the source model and the brain enclosing surface, a forward model was computed using the “single shell” method [21]. Subsequently, a Minimum Norm Estimate (MNE) inversion operator was computed using a pre-computed empty-room noise covariance matrix, regularized at a 10% level [22]. Prior to this analysis, the empty-room data, available in the Cam-CAN dataset for each experimental session, underwent identical preprocessing procedures as the human resting-state data. For further insights into preprocessing and MNE inversion operator computation, refer to [23].

C. MEG Functional Connectivity Estimation

For each participant, clean MEG resting state data were segmented in epochs of 2 seconds and projected to the central surface, using the pre-computed MNE inversion operator. Subsequently, the MEG sources were anatomically averaged onto 180 regions of interest (ROI) per hemisphere, totalling 360 ROIs of the Human Connectome Project Multi-Modal Parcellation atlas (HCP-MMP1) [24]. The averaging procedure involved identifying the predominant orientations of the dipoles within each ROI and aligning opposing dipoles through a process known as sign flipping to prevent spurious cancellations. This procedure yielded a single 2-second time series for each epoch per ROI, across all participants.

We computed the functional connectivity between ROIs in the alpha frequency band (8–13 Hz) using the Phase Locking Value (PLV) metric [25]:

$$PLV_{A,B} = \frac{1}{K} \sum_{k=1}^K \left| \frac{1}{T} \sum_{t=1}^T e^{-i(\phi_A(t)-\phi_B(t))} \right|, \quad (1)$$

where $\phi_A(t)$ and $\phi_B(t)$ are the instantaneous phases of the signals A and B at the instant t , T is the total number of time points per epoch, and K is the total number of epochs.

¹<https://neuro-jena.github.io/cat/>

This computation yielded a 360×360 connectivity matrix for each of the 587 participants. We selected the alpha frequency band (8–12 Hz) for this study based on its well-documented relevance to aging and neurodegenerative diseases, including AD. Abnormalities in the alpha band, such as decreased power and disrupted connectivity, have been consistently observed in individuals with AD, highlighting its potential as a sensitive marker of pathological changes [26]. Additionally, the alpha band exhibits the highest signal-to-noise ratio (SNR) among all frequency bands, characterized by a distinct power spectrum peak, making it a robust choice for reliable analysis. Furthermore, the alpha band has been extensively linked to cognitive processes like attention and memory, which are particularly affected by aging and neurodegeneration [27].

We chose the alpha band because numerous studies have consistently reported abnormalities in alpha band oscillations in individuals with AD.

Finally, to convert the connectivity matrices into graphs appropriate for FHNN processing, we set a threshold of 0.360 on the PLV values, thereby keeping only the top 5% of edges and discarding those below this cutoff (Fig. 1). This threshold was selected to preserve the most robust and meaningful functional connections, reflecting the overall global brain connectivity pattern while maintaining the scale-free (tree-like) nature of brain networks. Higher thresholds, which exclude more edges, can result in disconnected or fragmented graphs, thereby compromising the network’s integrity. On the other hand, lower thresholds retain an excessive number of weaker connections, making the graphs overly dense and shifting them away from their inherent scale-free structure. This shift would nullify the benefits of hyperbolic embeddings, which rely on hierarchical properties for effective representation. To ensure robustness, we tested various thresholds in our experiments and found that while the specific connectivity patterns varied, the overall trends and conclusions remained consistent across a range of thresholds.

D. Hyperbolic Embedding of MEG Brain Networks

1) Hyperbolic Geometry: Hyperbolic spaces are non-Euclidean spaces characterized by negative curvature ($K < 0$) as opposed to zero curvature in Euclidean spaces and positive curvature in spherical spaces. They are represented through various models, prominently the Poincaré disk model and the Lorentz (also known as hyperboloid) model, each offering distinct insights into their geometry and properties (Fig. 2). Recently, hyperbolic spaces have gained traction in representing tree-like graphs due to their capacity to represent hierarchical data effectively [28]. For instance, in a Poincaré model of hyperbolic space, a binary tree can be embedded with minimal distortion (see Fig. 2(b)).

Due to numerical instabilities inherent in the Poincaré model distance metric, recent studies have advocated the use of the Lorentz model [11], [28], [29]. In alignment with these works, we adopt the Lorentz model in our study. Geodesic distance in the Lorentz space can be computed by:

$$d_{\mathcal{L}}^K(\mathbf{x}, \mathbf{y}) = \frac{1}{\sqrt{|K|}} \cosh^{-1}(-K \langle \mathbf{x}, \mathbf{y} \rangle_{\mathcal{L}}), \quad (2)$$

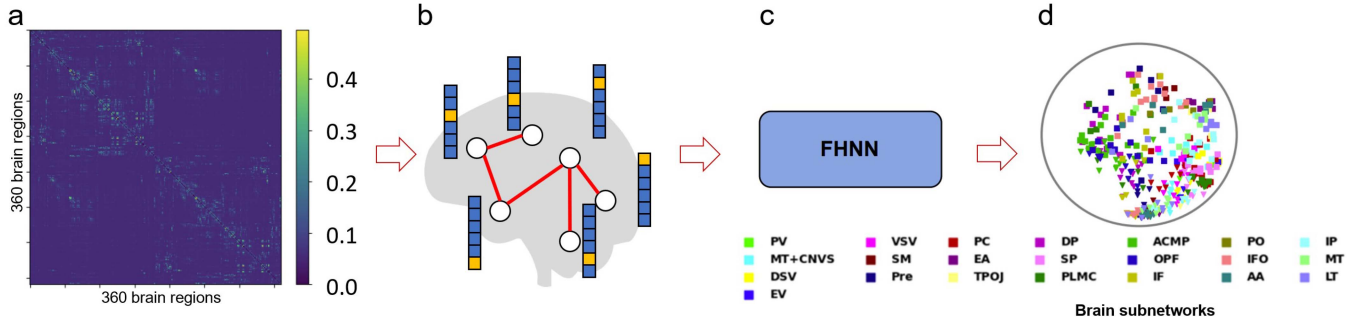


Fig. 1. Hyperbolic embedding framework of MEG brain networks. **(a)** MEG functional connectivity matrices, calculated based on phase locking values across all 360 regions of the HCP-MMP1 brain atlas, were thresholded to keep 5% of the connectivity values. **(b)** Brain networks with the remaining connections are illustratively visualized together with corresponding one-hot node features. **(c)** The brain data were fed to a fully hyperbolic neural network, yielding embeddings for each brain region of interest. **(d)** Embedded nodes are color-coded based on membership in each of the 22 subnetworks with similar functional specialization as in [24]. Shape indicates hemisphere: “□” for right hemisphere, “△” for left hemisphere. (PV: primary visual, VSV: ventral stream visual, PC: posterior cingulate, DP: dorsolateral prefrontal, ACMP: anterior cingulate and medial prefrontal, PO: posterior opercular, IP: inferior parietal, MT+CNVS: MT + complex and neighboring visual areas, SM: somatosensory and motor, EA: early auditory, SP: superior parietal, OPF: orbital and polar frontal, IFO: insular and frontal opercular, MT: medial temporal, DSV: dorsal stream visual, Pre: premotor, TPOJ: temporo-parieto-occipital junction, PLMC: paracentral lobular and mid cingulate, IF: inferior frontal, AA: auditory association, LT: lateral temporal, EV: early visual).

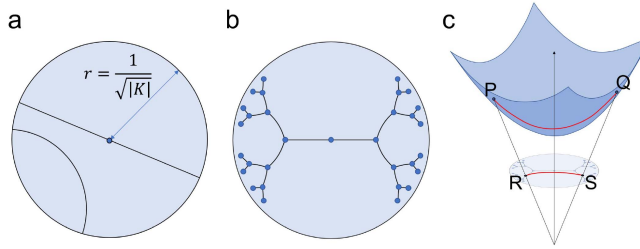


Fig. 2. Illustration of Poincaré and Lorentz hyperbolic models. **(a)** Poincaré space, represented as an n -dimensional open ball of fixed radius $r = 1/\sqrt{|K|}$. Geodesic lines are arcs bent towards the origin due to the negative curvature. **(b)** An example of a binary tree embedded in the Poincaré space, **(c)** Lorentz space, isomorphic to Poincaré space, depicted here with a projection onto a 2-dimensional Poincaré Disk. The projection mapping function acts as a generalization of stereographic projection to hyperbolic space.

where $K < 0$ is the hyperbolic space curvature, and $\langle \mathbf{x}, \mathbf{y} \rangle_{\mathcal{L}}$ is the Lorentzian inner product between points \mathbf{x} and \mathbf{y} .

Many essential operations in hyperbolic neural networks pose challenges, either being computationally intensive or lacking clear definitions within hyperbolic space. Consequently, these operations are typically handled through a hybrid approach. This involves translating features between the hyperbolic space \mathbb{L}_K^n and a tangent space $T_{\mathbf{x}}\mathbb{L}_K^n$ (a Euclidean subspace) around a hyperbolic point $\mathbf{x} \in \mathbb{L}_K^n$ and executing the operations within this tangent space. The transition between spaces is facilitated by logarithmic and exponential maps. Specifically, the logarithmic map, $\log_{\mathbf{x}}^K(\mathbf{y}) : \mathbb{L}_K^n \rightarrow T_{\mathbf{x}}\mathbb{L}_K^n$ maps a point $\mathbf{y} \in \mathbb{L}_K^n$ to the tangent space $T_{\mathbf{x}}\mathbb{L}_K^n$:

$$\log_{\mathbf{x}}^K(\mathbf{y}) = \frac{\operatorname{arccosh}(-K\langle \mathbf{x}, \mathbf{y} \rangle_{\mathcal{L}})}{\sqrt{K^2\langle \mathbf{x}, \mathbf{y} \rangle_{\mathcal{L}}^2 - 1}} (\mathbf{y} - |K|\langle \mathbf{x}, \mathbf{y} \rangle_{\mathcal{L}}\mathbf{x}). \quad (3)$$

Conversely, the exponential map $\exp_{\mathbf{x}}^K(\mathbf{z}) : T_{\mathbf{x}}\mathbb{L}_K^n \rightarrow \mathbb{L}_K^n$ plays an opposite role, lifting a point $\mathbf{z} \in T_{\mathbf{x}}\mathbb{L}_K^n$ from the tangent space

to the hyperbolic space \mathbb{L}_K^n :

$$\exp_{\mathbf{x}}^K(\mathbf{z}) = \cosh\left(\sqrt{|K|}\|\mathbf{z}\|_{\mathcal{L}}\right)\mathbf{x} + \frac{1}{\sqrt{|K|}} \sinh\left(\sqrt{|K|}\|\mathbf{z}\|_{\mathcal{L}}\right) \frac{\mathbf{z}}{\|\mathbf{z}\|_{\mathcal{L}}}, \quad (4)$$

where \mathbb{L}_K^n is the n -dimensional Lorentzian hyperbolic space (hyperboloid model) with negative curvature K , $T_{\mathbf{x}}\mathbb{L}_K^n$ is the tangent space centered at \mathbf{x} , $\mathbf{z} \in T_{\mathbf{x}}\mathbb{L}_K^n$, and $\|\mathbf{z}\|_{\mathcal{L}} = \langle \mathbf{z}, \mathbf{z} \rangle_{\mathcal{L}} = -z_0^2 + \sum_{i=1}^{n-1} z_i^2$. Studies typically set $\mathbf{x} = \mathbf{o} = (\sqrt{-1/K}, 0, \dots, 0)$ to establish exponential and logarithmic maps between hyperbolic space and the tangent space at the origin.

2) Fully Hyperbolic Neural Network: Previous hyperbolic neural network models primarily formalized operations within intermediate tangent spaces, making them not fully hyperbolic. The logarithmic and exponential maps required to transition to the tangent space involve a series of hyperbolic and inverse hyperbolic functions, whose compositions are complex and often extend to infinity, which significantly undermine the stability of the models. However, recent advancements have led to the development of fully hyperbolic neural networks (FHNN) [15]. This innovation was achieved by relaxing certain restrictions in Lorentz transformations that complicate computations and optimizations, and by designing network layers with feature transformations that inherently preserve data within the Lorentz space. This Lorentz model variant makes it possible to directly formalize operations in hyperbolic space, obviating the need for intermediate tangent spaces via exponential and logarithmic maps. Additionally, the Lorentz model, although harder to visualize, is more numerically stable than the Poincaré model [29].

Further, to formalize operations such as attention and aggregation directly in hyperbolic space, the FHNN model leverages a proof by Law et al. [29], which shows that, with squared Lorentzian distance defined as $d_{\mathcal{L}}^2(\mathbf{a}, \mathbf{b}) = \frac{2}{K} - \langle \mathbf{a}, \mathbf{b} \rangle_{\mathcal{L}}$, the

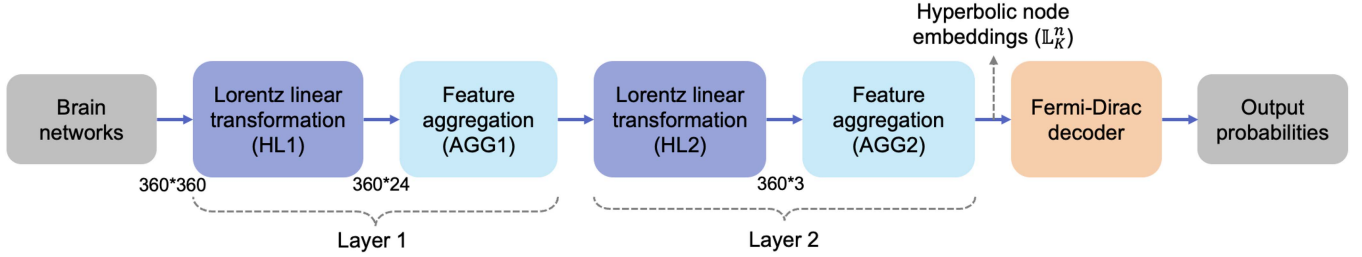


Fig. 3. Main architecture of the FHNN model for the link prediction task in MEG brain networks. Each input high-dimensional MEG brain network of size 360×360 is first projected to a low-dimensional hyperbolic Lorentzian manifold (\mathbb{L}_K^n , where $K < 0$ is the curvature, n is the dimensionality of manifold) with learned “continuous hierarchies” through two consecutive projection layers with output feature sizes 360×24 and 360×3 , respectively. Each projection layer contains two main operations: hyperbolic (or Lorentz) linear transformation (HL) and feature aggregation (AGG). The Fermi-Dirac decoder is then used to decode the edge probabilities for link prediction from the learned node hyperbolic embeddings.

centroid induced by this distance has a closed-form given by:

$$\mu = \frac{\sum_{j=1}^{|P|} \nu_j \mathbf{x}_j}{\sqrt{|K|} \|\sum_{j=1}^{|P|} \nu_j \mathbf{x}_j\|_L}, \quad (5)$$

where P is the point set $P = \{\mathbf{x}_1, \dots, \mathbf{x}_{|P|}\}$, with \mathbf{x}_i being the i -th node’s hyperbolic embedding representation and ν_i being its weight. This calculation is much faster than current algorithmic implementations like the Fréchet mean in standard hyperbolic spaces [30] [31]. The FHNN centroid is also better than the Einstein midpoint since the latter requires mapping back and forth between the Klein and Poincaré models in order to compute the centroid, potentially leading to information loss [15], [32].

Our adapted FHNN architecture is illustrated in Fig. 3 and can be summarized into three parts: feature transformation, neighborhood aggregation, and non-linear activation. The feature transformation corresponds to a Lorentz linear layer, while the closed-form centroid of neighboring node features defined before is used for neighborhood aggregation. Non-linearity is integrated into the Lorentz linear layer without the need for an explicit non-linear activation function. Below we discuss the model’s individual components.

Model Input Features: In graph neural networks, node features capture additional information associated with each node in a graph. In absence of other relevant information, we used a common approach: one-hot identity vectors.

Fully Hyperbolic Linear Layer – Feature Transform: The hyperbolic linear layer was devised to automatically preserve data in the Lorentz space, and includes dropout, bias and normalization:

$$\mathbf{y} = \text{HL}(\mathbf{x}) = \begin{bmatrix} \sqrt{\|\phi(\mathbf{Wx}, \mathbf{v})\|^2 - 1/K} \\ \phi(\mathbf{Wx}, \mathbf{v}) \end{bmatrix}, \quad (6)$$

where $\phi(\mathbf{Wx}, \mathbf{v}) = \frac{\lambda \sigma(\mathbf{v}^\top \mathbf{x} + b) + \epsilon}{\|\mathbf{W}\text{dropout}(\mathbf{x})\|} \mathbf{W}\text{dropout}(\mathbf{x})$, $\mathbf{x} \in \mathbb{L}_K^n$, $\mathbf{v} \in \mathbb{R}^{n+1}$, $\mathbf{W} \in \mathbb{R}^{m \times (n+1)}$, σ is the sigmoid function, b' is a bias term, and $\lambda > 0$ controls the scaling range.

Fully Hyperbolic Aggregation Layer: Relying on the centroid induced by the squared Lorentzian distance [29] ((5)), the aggregation layer in the FHNN uses the following equation:

$$\mathbf{h} = \text{AGG}(\mathbf{A}, \mathbf{y}) = \frac{\mathbf{Ay}}{\sqrt{\|\mathbf{Ay}\|_L}}, \quad (7)$$

where \mathbf{A} denotes the adjacency matrix of the MEG brain network, and \mathbf{y} is the layer input.

Link Prediction: Our FHNN model was trained using a link prediction task, which is a common evaluation method in network science [28]. In this task, we aim to predict the presence or absence of edges within a network. Specifically, we divided the entire dataset of 587 MEG connectivity matrices into three sets: 70% for training, 20% for validation, and 10% for testing. To perform link prediction, we masked a set of edges (and a matching number of non-edges) from the graph and trained the model to predict whether each edge should exist. The model’s performance was evaluated based on its ability to correctly predict these connections. The Fermi-Dirac decoder translated the proximity of node embeddings in hyperbolic space into probabilities for edge existence [28]. The probability score of a link (or edge) between two nodes i and j at the output layer L is defined as:

$$p((i, j) \in \mathcal{E} | \mathbf{x}_i^L, \mathbf{x}_j^L) = \frac{1}{e^{(d_{KL}(\mathbf{x}_i^L, \mathbf{x}_j^L)^2 - r)/t} + 1}. \quad (8)$$

That is, an edge between two nodes is predicted to exist according to a sigmoidal transformation of the hyperbolic distance between the node embeddings. The hyperparameters r and t control the inflection point and steepness of the sigmoid function, and were set as $r = 2$ and $t = 1$. Finally, the link prediction loss function employed in our model is a margin loss:

$$L_{\text{margin}}(\mathbf{s}, y) = \max(m + \max(\mathbf{s}_{-y}) - \mathbf{s}_y, 0), \quad (9)$$

where m is the margin, \mathbf{s} is the output vector of predicted probabilities or scores for each category (in this case, there are two categories: edge exists vs. does not), y is the label, \mathbf{s}_y is the component of the correct label, and \mathbf{s}_{-y} is the vector composed of all other components corresponding to categories other than the label.

E. Parameter Settings and Model Training

Graph neural networks, including FHNNs, often benefit from shallower architectures to prevent over-smoothing, where node representations become indistinguishable after aggregating information from too many layers. In our case, the small size of

the 360×360 brain graphs allowed us to use two layers without over-smoothing (Fig. 3). The input features, initially sized 360×360 , were reduced to 360×24 in the first layer and then to 360×3 in the second layer. The choice of a smaller embedding size (24) minimized overparameterization while maintaining model accuracy in link prediction. An output embedding size of 3 was selected based on previous studies, which indicated that larger embedding sizes lead to diminishing returns in link prediction performance while increasing the costs of interpretability and overparameterization [30]. We normalized the features and row-normalized the adjacency matrix.

Graph neural networks (GNNs), including FHNNs, often benefit from shallower architectures to prevent over-smoothing, where node representations become indistinguishable after aggregating information from too many layers. In our case, the small size of the 360×360 brain graphs allowed us to use only two layers without over-smoothing: a 360×24 layer and a 24×3 layer. The choice of a smaller embedding size (24) minimizes overparameterization while maintaining model accuracy in link prediction.

The parameters of the FHNN consisted of the weights and biases for the feature transformation layer, as defined in (6). In the first hyperbolic layer, the weight matrix had dimensions 360×24 , with a corresponding bias vector of size 24×1 . In the second layer, the weight matrix was 24×3 , and the bias vector was 3×1 . All weight parameters were randomly initialized using Xavier initialization to provide an optimal starting point for training.

The hyperparameters for the FHNN embedding framework were configured as follows: Optimizer hyperparameters included a maximum of 300 epochs, an early stopping criterion at 150 epochs, gradient clipping set to 0.1, a learning rate of 0.025, and weight decay of 0.001. Data handling was controlled with a hyperparameter of batch size equal to 64. Model hyperparameters included a curvature value $C=1$, Fermi-Dirac encoder values $r=2$ and $t=1$, and a margin of 2 for the link prediction margin loss function. The choice of hyperparameters were based on a combination of prior studies [15] and grid search to optimize performance. The grid search explored learning rates [0.01, 0.025, 0.05, 0.1], dropout rates [0.0, 0.25, 0.5, 0.75], and gradient clip values [0.01, 0.1, 1, 10]. The best metrics — an average precision and ROC AUC score of approximately 70% — were achieved with a learning rate of 0.025, a dropout rate of 0.25, and gradient clipping at 0.1. Curvature and Fermi-Dirac encoder values and the margin hyperparameter were adopted from prior work [15]. Training was conducted using the Riemannian Adam optimizer [33].

III. RESULTS

A. Link Prediction Results

The FHNN model was trained on a link prediction task [15] to generate hyperbolic node embeddings, capturing both the local and global geometric properties of the MEG brain networks. The training utilized a margin loss function (9) and was conducted over a maximum of 300 epochs with early stopping at 150 epochs. The model achieved a test loss of 1.738, along

with strong performance metrics: test accuracy of 0.826, test precision of 0.837, and test AUC-ROC of 0.895. These results underscore the FHNN model's ability to produce high-quality hyperbolic embeddings that preserve the intricate geometric structure of the brain networks.

B. Alterations of Brain Network Hierarchy Across Age

Hyperbolic embeddings are powerful tools for representing hierarchical data due to the natural alignment between the geometric properties of hyperbolic space and the structural characteristics of hierarchies. In hyperbolic space, hierarchical relationships become more pronounced: central nodes often represent higher-level categories, while peripheral nodes correspond to subcategories. This is illustrated in Fig. 2(b), where nodes near the root of the tree are placed close to the origin, and nodes further from the root are situated farther out. Leveraging this property, we calculated the hyperbolic radius of each brain region as an indicator of its position within the overall brain hierarchy. This metric, computed for each brain region across the 587 participants of the Cam-CAN database, allowed us to characterize subtle hierarchical organizational changes in various brain subnetworks associated with the aging process. In our study, we used the van Essen HCP multimodal atlas, which comprises 360 brain regions that were subsequently grouped into 22 subnetworks, organized according to their structural properties, functional task-related profiles, and functional connectivity patterns [24].

We estimated the average hyperbolic radius for brain regions within each of 22 brain subnetworks and across participants of the same decade (Table I), as depicted in Fig. 4. The findings suggest a consistent increase in the hyperbolic radius across most of the 22 brain subnetworks over the decades, indicative of a diminishing hierarchical significance over time. Notably, certain subnetworks exhibit more rapid changes over time than others.

To investigate further, we fitted a linear regression model to the 7-decade hyperbolic radius data points for each brain subnetwork, obtaining a slope value that indicates the alteration of the subnetwork's hyperbolic radius across age (Fig. 5). Our findings reveal statistically significant increases in hyperbolic radius within the majority of the brain subnetworks. Notably, primary cortical areas, including the primary visual, early visual, somatosensory, and motor subnetworks, exhibit the most prominent changes. Conversely, several other subnetworks demonstrate more gradual alterations, with brain subnetworks such as early auditory and posterior opercular exhibiting near-zero slopes across age decades. Additionally, we observed that brain subnetworks with a smaller overall hyperbolic radius tend to have higher slopes, indicating a faster reduction in hierarchy within regions that initially have a high hierarchical organization.

The slopes of the age-related hyperbolic radius changes are visualized on a smoothed cortical manifold for the 360 brain regions comprising the HCP-MMP1 atlas [24] (Fig. 6). Additionally, we illustrate the hyperbolic embeddings of two brain subnetworks with contrasting aging trajectories in Fig. 7. The

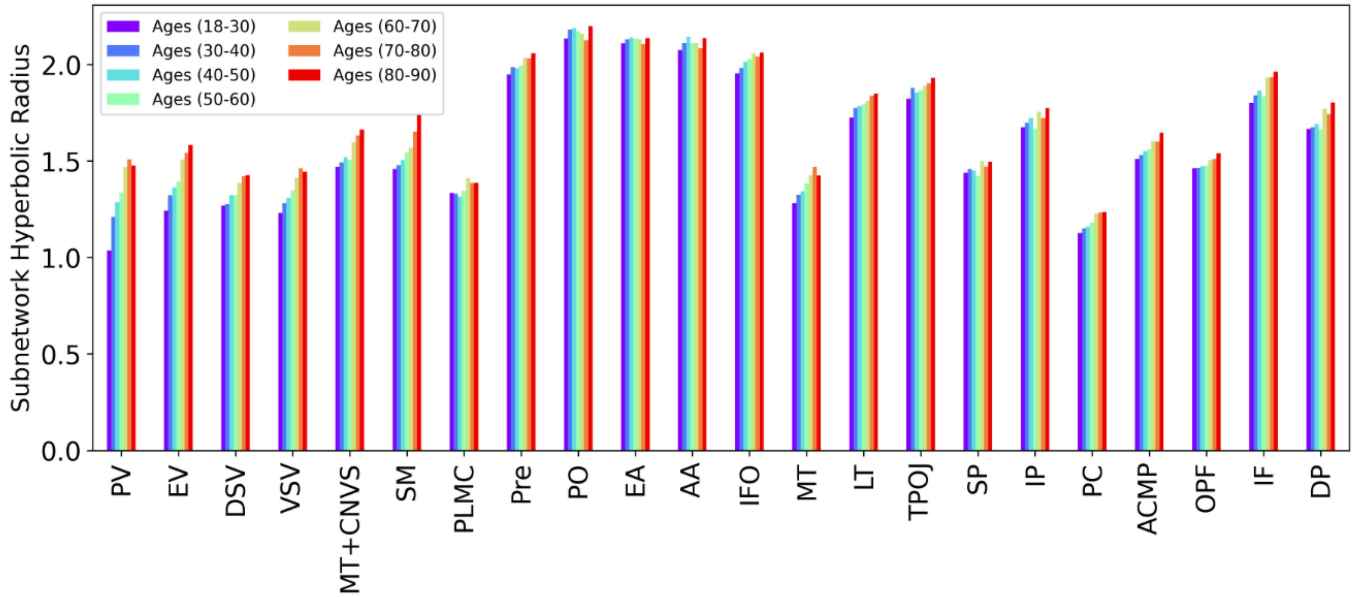


Fig. 4. Hyperbolic radius changes for each of the 22 brain subnetworks across 7 age decades. The full subnetwork names are provided in Fig. 1.

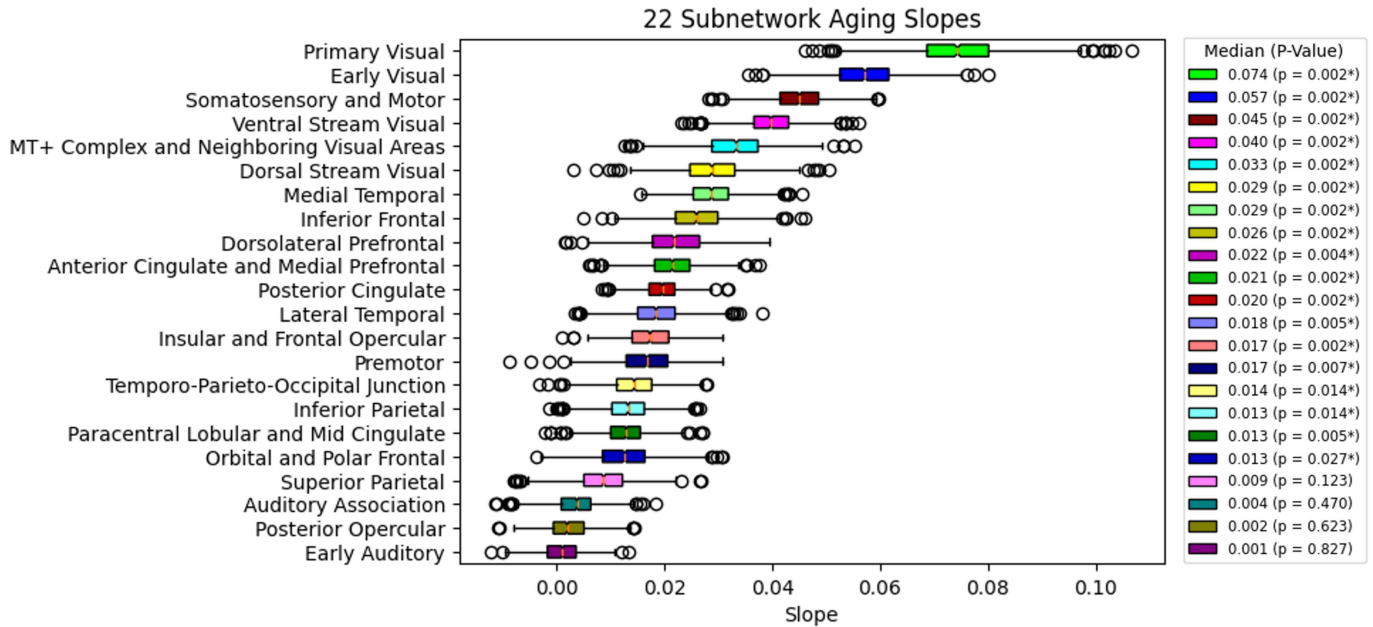


Fig. 5. Slope of hyperbolic radius change for each of the 22 brain subnetworks. Each slope was computed by fitting a linear regression model to the 7-decade hyperbolic radius data of the corresponding subnetwork. Box plots were constructed using the distribution of 1000 bootstrap samples from the 587 Cam-CAN participants. P-values were calculated using 1000 permutation samples by randomly shuffling the subject's age labels and recomputing the slopes for each permutation sample. These p-values were then adjusted for multiple comparisons using false discovery error rate. Statistically significant p-values at a 5% level are indicated with a star (*).

embeddings of brain regions within the early visual subnetwork, which exhibits a high slope, are shown for both the 1st decade (18–30 years) and the 7th decade (80–90 years). In the 7th decade, these embeddings have shifted towards the periphery, reflecting a pronounced increase in the overall hyperbolic radius and thus a decrease in brain network hierarchy. For contrast, we also present the hyperbolic embeddings of areas within the early auditory subnetwork, a region with a nearly flat slope and stable hyperbolic radius from the 1st to the 7th decade. Note that

the hyperbolic embeddings are isomorphically projected from the Lorentz space, the native space of the FHNN model, to the Poincaré disk for easier visualization.

C. Age Prediction With Hyperbolic Radius

Deep learning is highly effective at automatically discovering informative features from data for downstream tasks. We hypothesized that hyperbolic radii, which reflect the automatically

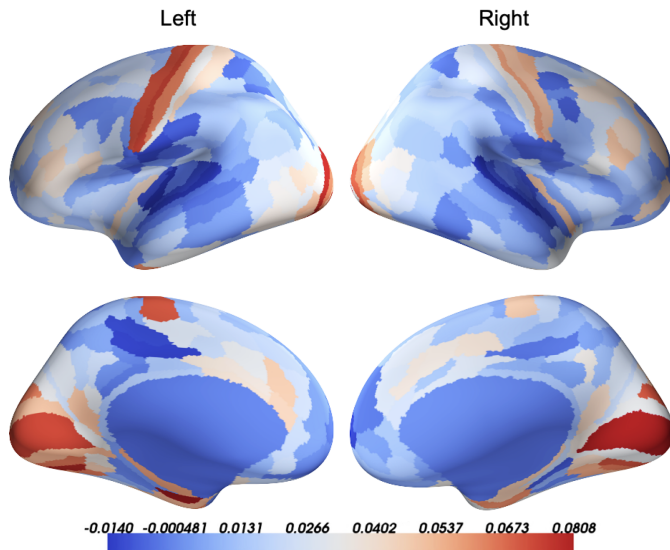


Fig. 6. Visualization of age-related slopes of hyperbolic radius change for the 360 brain regions defined in the HCP-MMP1 atlas [24].

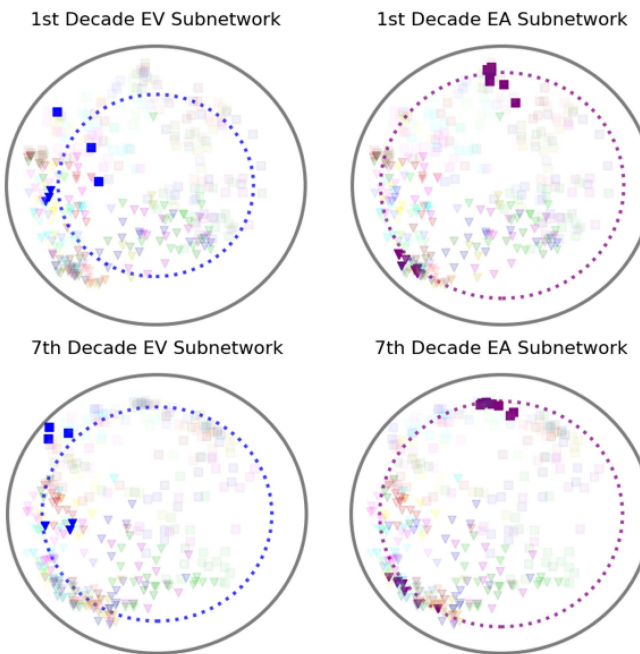


Fig. 7. Hyperbolic embeddings of the 360 brain regions for participants aged in the 1st decade (18–30 years) and 7th decade (80–90 years). Two subnetworks, the *early visual* and *early auditory*, are highlighted, while the rest are faded. Early visual areas show significant increases in hyperbolic radius, whereas early auditory areas remain stable over time. Individual points represent different brain regions, with shapes indicating the hemisphere ("□" for right hemisphere, "△" for left hemisphere) and colors indicating subnetwork membership, consistent with Fig. 1.

detected hierarchy of each brain region from the FHNN model, would serve as more powerful features than traditional hand-crafted graph-theoretic features that also reflect node importance, such as closeness centrality and betweenness centrality.

To evaluate, we assessed the effectiveness of using the hyperbolic radius of the 360 brain regions versus standard graph-theoretic measures for the downstream task of age prediction.

For comparison, we computed eight commonly used standard graph-theoretic measures—shortest path length, efficiency, clustering coefficient, degree centrality, Katz centrality, closeness centrality, betweenness centrality, and average neighbor degree—for the MEG brain networks of the 587 subjects. To ensure a robust and comprehensive comparison, we tested three regression methods (AdaBoost, Ridge Regression, and Random Forest) with features consisting of the hyperbolic radii or the standard graph measures. We also compared performance when concatenating both features. Model fitting was performed using the same 70/30% train-test split as in the FHNN training procedure to ensure generalizability.

The corresponding age prediction performance, measured by Mean Absolute Error (MAE), is shown in Table II. We observe that the hyperbolic radius outperformed all standard graph-theoretic measures, achieving lower MAE across all the three different regression models. Further, by concatenating hyperbolic radius as an additional regression feature to the standard graph measures, all three regression models improved performance relative to using standard graph measures alone. Our findings validate that hyperbolic node embeddings are rich low-dimensional representations of MEG brain networks that encode more powerful age-related information in brain networks than standard graph measures.

The implementation of our adapted FHNN model for MEG brain network embeddings can be found in https://github.com/Hramir/age_prediction. Note, we trained FHNNs on small 360×360 brain graphs, enabling efficient optimization on modest hardware like a CPU. While not tested on large datasets, FHNNs are expected to scale effectively, similar to other graph convolutional architectures, especially when integrated into specialized libraries.

IV. DISCUSSION

We developed a novel hyperbolic MEG brain network embedding framework based on the FHNN architecture [15], and proposed using the hyperbolic radii of the node embeddings as features to study aging trajectories. Our findings revealed that hyperbolic embeddings are powerful signatures of the aging brain, surpassing traditional graph theoretic measures in capturing age-related information from MEG brain networks.

Our findings revealed that a significant number of subnetworks underwent a reduction in hierarchy during aging, with some exhibiting gradual changes while others experienced rapid transformations. Similar trends have been previously observed using graph-theoretical measures on resting state fMRI [34] and MEG data [35]. Despite its potential relevance as a diagnostic marker for neurodegenerative disorders, the general trend of brain-network reorganization during healthy aging and its dependence on specific brain subnetworks remains poorly understood. Our novel metric, directly related to the loss of hierarchical organization as quantified by the hyperbolic radius, may offer greater efficiency and interpretability compared to classical graph-theoretical measures.

Our findings align with and build upon previous research exploring hierarchical changes in brain networks associated

TABLE II
MEAN ABSOLUTE ERROR (%) RESULTS FOR AGE PREDICTION WITH DIFFERENT REGRESSION MODELS AND FEATURES (THE MAE DIFFERENCES BETWEEN APPLYING INDIVIDUAL MEASURES AND COMBINED EACH FEATURE WITH HYPERBOLIC RADIUS FEATURE ARE SHOWN IN PARENTHESES.)

Graph Measure Feature	Individual Measures			Measures Combined with Hyperbolic Radius		
	Ada-Boost	Ridge	Random Forest	Ada-Boost	Ridge	Random Forest
Shortest Path Length	15.24	14.83	15.36	13.16 (-2.08)	13.19 (-1.64)	13.29 (-2.07)
Efficiency	14.07	13.81	14.03	13.05 (-1.02)	13.26 (-0.55)	13.17 (-0.86)
Clustering	13.91	14.92	14.23	12.74 (-1.17)	13.08 (-1.84)	12.99 (-1.24)
Degree Centrality	13.85	13.62	13.92	12.73 (-1.12)	13.12 (-0.50)	12.78 (-1.14)
Katz Centrality	15.29	15.88	15.24	13.57 (-1.72)	13.77 (-2.11)	13.31 (-1.93)
Closeness Centrality	14.10	14.05	14.37	12.9 (-1.20)	13.30 (-0.75)	12.99 (-1.38)
Betweenness Centrality	14.08	15.58	14.10	12.95 (-1.13)	13.4 (-2.18)	12.79 (-1.31)
Average Neighbor Degree	14.48	14.19	14.50	12.76 (-1.72)	13.42 (-0.77)	12.96 (-1.54)
Hyperbolic Radius	13.01	13.16	13.00	—	—	—

with aging. Prior studies have established that aging is associated with reduced network segregation, decreased global efficiency, and alterations in the hierarchical organization of functional brain networks. For example, research on whole-brain connectivity patterns has shown that aging particularly affects the default mode network (DMN) and sensory-motor networks, leading to reduced segregation and reorganization of functional hierarchies [36]. Similarly, age-related declines in structural integrity have been linked to diminished functional communication and disrupted hierarchical organization [37]. Lifespan-wide morphometric analyses emphasize the maturation of the DMN during adolescence and its reconfiguration in older age [38], while other studies report a shift in functional connectivity toward primary sensory-motor regions, rather than the DMN, in older adults, reflecting a reorganization of hub systems [39]. Expanding on these findings, our work introduces a novel approach that embeds functional brain connectivity graphs into a Lorentz model of hyperbolic space, enabling explicit capture of hierarchical changes. By leveraging the hyperbolic radius metric, we provide a unique perspective on aging-related reorganization of functional brain hierarchies, complementing traditional graph-theoretic metrics.

While the most pronounced changes in the slope of the hyperbolic radius were concentrated in the visual, somatosensory, and motor areas, we also observed significant positive slopes across a wide range of brain regions. Notably, this included prefrontal areas such as the Dorsolateral Prefrontal Cortex (DP) and the Anterior Cingulate and Medial Prefrontal Cortex (ACMP). This aligns with the hierarchical organization of the prefrontal cortex at the network level [40] and its critical role in modulating cognitive functions that change with age [41]. Age-related functional changes in the prefrontal cortex have been linked to declines in memory performance [42] and alterations in cognitive and motor functions [43].

We introduced the hyperbolic radius as a novel metric for quantifying hierarchical organization in MEG brain networks, building on the intrinsic geometry of hyperbolic space, where distance from the origin encodes hierarchical relationships. This metric aligns with neurobiological principles of scale-free brain networks with central hubs and specialized regions [44]. While theoretical studies support its use [11], [28], further empirical validation is needed to confirm its neurobiological relevance. Our results show that hyperbolic embeddings outperform

traditional graph-theoretic measures in capturing age-related changes, highlighting the potential of the hyperbolic radius as a robust and interpretable marker of brain network reorganization during aging. Future research should explore its correlation with biological markers and cognitive performance to strengthen its utility.

While this study focused on the alpha frequency band (8–12 Hz) due to its robustness and established relevance to aging and neurodegenerative diseases, other frequency bands, such as theta (4–8 Hz) and beta (13–30 Hz), may also demonstrate age-related hierarchical changes. For instance, research has shown that aging is associated with increased theta activity and altered beta-band connectivity, which are linked to cognitive decline and changes in functional brain networks [45]. Future research could explore these additional bands to provide a more comprehensive understanding of how functional connectivity evolves across different frequency domains during aging.

Although clinical applications were not the primary focus of this study, our framework holds considerable promise for enhancing the understanding and prediction of neurodegenerative diseases. These conditions often involve subtle neuropathological processes that begin many years before overt clinical symptoms emerge, including cortical atrophy and disruptions in network connectivity. For example, AD is marked by specific alterations in oscillatory activity—particularly in the alpha and beta bands—as well as decreased local amplitude and node-to-global connectivity that differ from normal aging patterns [46]. Furthermore, hierarchical disruptions in network organization, reflected in altered graph-theoretic properties such as modularity, segregation, and integration, underscore the vulnerability of brain networks in neurodegenerative conditions [47].

Our study was designed to characterize normal aging trajectories, thereby providing a critical baseline against which early pathological changes can be detected. In this context, the hyperbolic radius metric—quantifying hierarchical alterations in brain network organization—shows substantial potential as a sensitive biomarker for early neurodegenerative processes. Given that disruptions in functional connectivity and hierarchical organization are established precursors to cognitive decline, our method facilitates direct comparisons between patient data and normative trajectories derived from healthy individuals, pinpointing emergent deviations. Additionally, modeling hierarchical network changes offers a novel lens on how clinical

conditions reshape brain organization. For instance, hyperbolic embeddings could help localize the specific subnetworks or regions where hierarchical disruptions are most pronounced, providing essential insights into disease progression and identifying the most vulnerable neural systems.

By refining our understanding of hierarchical network organization, the hyperbolic radius could catalyze the development of sensitive biomarkers and predictive tools for neurodegenerative diseases, supporting earlier detection and intervention at the time when therapies are most beneficial [48], [49].

V. CONCLUSION

Our hyperbolic MEG brain network embedding framework effectively transformed complex high-dimensional MEG brain networks into lower-dimensional hyperbolic representations, facilitating brain hierarchy analysis across age. Our findings revealed that a considerable number of brain subnetworks exhibited a reduction in hierarchy during aging.

In contrast to other machine learning models, our methods generate hyperbolic node embeddings that offer straightforward interpretation through visualization in the Poincaré Disk. These embeddings carry tangible meaning, demonstrated by the hyperbolic radius serving as a measure of hierarchical brain organization. Consequently, one can readily distinguish abnormal brain networks from normal ones with greater interpretability compared to models lacking a direct association between internal representations and physiological significance.

Overall, our study presented the first evaluation of hyperbolic embeddings in MEG brain networks across age, introduced a novel neural embedding measure of brain hierarchy, and used this measure to highlight aging trajectories in the large cohort of the Cam-CAN dataset. Our approach has the potential to deepen our understanding of the aging brain, help in delineating normative brain aging trajectories, and pinpoint deviations indicative of neurodegenerative disorders, such as Alzheimer's disease.

REFERENCES

- [1] C. R. Jack et al., "Tracking pathophysiological processes in Alzheimer's disease: An updated hypothetical model of dynamic biomarkers," *Lancet Neurol.*, vol. 12, no. 2, pp. 207–216, 2013.
- [2] J. R. Sims et al., "Donanemab in early symptomatic Alzheimer disease: The TRAILBLAZER-ALZ 2 randomized clinical trial," *Jama*, vol. 330, no. 6, pp. 512–527, 2023.
- [3] W. S. Liang, L. H. Goetz, and N. J. Schork, "Assessing brain and biological aging trajectories associated with Alzheimer's disease," *Front. Neurosci.*, vol. 16, 2022, Art. no. 1036102.
- [4] M. Xu, D. L. Sanz, P. Garces, F. Maestu, Q. Li, and D. Pantazis, "A graph Gaussian embedding method for predicting Alzheimer's disease progression with MEG brain networks," *IEEE Trans. Biomed. Eng.*, vol. 68, no. 5, pp. 1579–1588, May 2021.
- [5] C. Baker et al., "Hyperbolic graph embedding of MEG brain networks to study brain alterations in individuals with subjective cognitive decline," *IEEE J. Biomed. Health Inform.*, vol. 28, no. 12, pp. 7357–7368, Dec. 2024.
- [6] D. Pantazis, M. Fang, S. Qin, Y. Mohsenzadeh, Q. Li, and R. M. Cichy, "Decoding the orientation of contrast edges from MEG evoked and induced responses," *NeuroImage*, vol. 180, pp. 267–279, 2018.
- [7] M. Rubinov and O. Sporns, "Complex network measures of brain connectivity: Uses and interpretations," *Neuroimage*, vol. 52, no. 3, pp. 1059–1069, 2010.
- [8] F. Bloch, M. O. Jackson, and P. Tebaldi, "Centrality measures in networks," *Social Choice Welfare*, vol. 61, no. 2, pp. 413–453, 2023.
- [9] V. Menon, "Large-scale brain networks and psychopathology: A unifying triple network model," *Trends Cogn. Sci.*, vol. 15, no. 10, pp. 483–506, 2011.
- [10] G. Rosenthal et al., "Mapping higher-order relations between brain structure and function with embedded vector representations of connectomes," *Nature Commun.*, vol. 9, no. 1, pp. 1–12, 2018.
- [11] I. Chami, Z. Ying, C. Ré, and J. Leskovec, "Hyperbolic graph convolutional neural networks," in *Proc. 33rd Int. Conf. Neural Inf. Process. Syst.*, 2019, pp. 4868–4879.
- [12] W. Peng, T. Varanka, A. Mostafa, H. Shi, and G. Zhao, "Hyperbolic deep neural networks: A survey," *IEEE Trans. pattern Anal. Mach. Intell.*, vol. 44, no. 12, pp. 10023–10044, Dec. 2022.
- [13] A. Longhena, M. Guillemaud, and M. Chavez, "Detecting local perturbations of networks in a latent hyperbolic embedding space," *Chaos: Interdiscipl. J. Nonlinear Sci.*, vol. 34, no. 6, 2024, Art. no. 063117.
- [14] A. Longhena, M. Guillemaud, F. D. V. Fallani, R. Migliaccio, and M. Chavez, "Hyperbolic embedding of brain networks detects regions disrupted by neurodegeneration in Alzheimers disease," *Phys. Rev. E*, Feb. 2025.
- [15] W. Chen et al., "Fully hyperbolic neural networks," in *Proc. 60th Annu. Meet. Assoc. Comput. Linguistics (Volume 1: Long Papers)*, Dublin, Ireland, 2022, pp. 5672–5686.
- [16] J. R. Taylor et al., "The Cambridge centre for ageing and neuroscience (CAM-CAN) data repository: Structural and functional MRI, MEG, and cognitive data from a cross-sectional adult lifespan sample," *Neuroimage*, vol. 144, pp. 262–269, 2017.
- [17] M. F. Folstein, S. E. Folstein, and P. R. McHugh, "Mini-mental state. A practical method for grading the cognitive state of patients for the clinician," *J. Psychiatr.*, vol. 12, pp. 189–198, 1975.
- [18] R. Oostenveld, P. Fries, E. Maris, and J.-M. Schoffelen, "Fieldtrip: Open source software for advanced analysis of MEG, EEG, and invasive electrophysiological data," *Comput. Intell. Neurosci.*, vol. 2011, pp. 1–9, 2011.
- [19] S. Taulu and J. Simola, "Spatiotemporal signal space separation method for rejecting nearby interference in meg measurements," *Phys. Med. Biol.*, vol. 51, no. 7, p. 1759, 2006.
- [20] T.-W. Lee, M. Girolami, and T. J. Sejnowski, "Independent component analysis using an extended infomax algorithm for mixed subGaussian and superGaussian sources," *Neural Computation*, vol. 11, no. 2, pp. 417–441, 1999.
- [21] G. Nolte, "The magnetic lead field theorem in the quasi-static approximation and its use for magnetoencephalography forward calculation in realistic volume conductors," *Phys. Med. Biol.*, vol. 48, no. 22, 2003, Art. no. 3637.
- [22] R. Ilmoniemi and J. Sarvas, *Brain Signals: Physics and Mathematics of MEG and EEG*. London, U.K.: Mit Press, 2019.
- [23] D. Tabarelli, A. Brancaccio, C. Zrenner, and P. Belardinelli, "Functional connectivity states of alpha rhythm sources in the human cortex at rest: Implications for real-time brain state dependent EEG-TMS," *Brain Sci.*, vol. 12, no. 3, 2022, Art. no. 348.
- [24] M. F. Glasser et al., "A multi-modal parcellation of human cerebral cortex," *Nature*, vol. 536, pp. 171–178, 2016.
- [25] J.-P. Lachaux, E. Rodriguez, J. Martinerie, and F. J. Varela, "Measuring phase synchrony in brain signals," *Hum. Brain Mapping*, vol. 8, no. 4, pp. 194–208, 1999.
- [26] M. E. López et al., "Alpha-band hypersynchronization in progressive mild cognitive impairment: A magnetoencephalography study," *J. Neurosci.*, vol. 34, no. 44, pp. 14551–14559, 2014.
- [27] W. Klimesch, "Alpha-band oscillations, attention, and controlled access to stored information," *Trends Cogn. Sci.*, vol. 16, no. 12, pp. 606–617, 2012.
- [28] M. Nickel and D. Kiela, "Poincaré embeddings for learning hierarchical representations," in *Proc. 31st Int. Conf. Neural Inf. Process. Syst.*, pp. 6341–6350, 2017.
- [29] M. T. Law, R. Liao, J. Snell, and R. S. Zemel, "Lorentzian distance learning for hyperbolic representations," in *Proc. 36th Int. Conf. Mach. Learn.*, 2019, pp. 3672–3681.
- [30] C. Baker, I. Suarez-Mendez, F. Maestu, M. Xu, and D. Pantazis, "Hyperbolic graph embedding of MEG brain networks to study brain alterations in individuals with subjective cognitive decline," *IEEE J. Biomed. Health Informat.*, vol. 28, no. 12, pp. 7357–7368, Dec. 2024.
- [31] A. Lou, I. Katsman, Q. Jiang, S. Belongie, S.-N. Lim, and C. D. Sa, "Differentiating through the Fréchet mean," in *Proc. 37th Int. Conf. Mach. Learn.*, 2020, pp. 6393–6403.
- [32] J. Dai, Y. Wu, Z. Gao, and Y. Jia, "A hyperbolic-to-hyperbolic graph convolutional network," in *Proc. IEEE/CVF Conf. Comput. Vis. Pattern Recognit.*, 2021, pp. 154–163.

- [33] M. Kochurov, R. Karimov, and S. Kozlukov, “Geoopt: Riemannian optimization in PyTorch,” 2020, *arXiv:2005.02819*.
- [34] H. A. Deery, R. Di Paolo, C. Moran, G. F. Egan, and S. D. Jamadar, “The older adult brain is less modular, more integrated, and less efficient at rest: A systematic review of large-scale resting-state functional brain networks in aging,” *Psychophysiol.*, vol. 60, no. 1, 2023, Art. no. e14159.
- [35] N. Coquelet et al., “Changes in electrophysiological static and dynamic human brain functional architecture from childhood to late adulthood,” *Sci. Rep.*, vol. 10, no. 1, 2020, Art. no. 18986.
- [36] X. Wang, C.-C. Huang, S.-J. Tsai, C.-P. Lin, and Q. Cai, “The aging trajectories of brain functional hierarchy and its impact on cognition across the adult lifespan,” *Front. Aging Neurosci.*, vol. 16, 2024, Art. no. 1331574.
- [37] H. Zhang, P. Cao, H. K. Mak, and E. S. Hui, “The structural-Functional-connectivity coupling of the aging brain,” *GeroScience*, vol. 46, pp. 3875–3887, 2024.
- [38] X. Qian and J. H. Zhou, “Imaging lifespan brain structural growth: From region, to connectome, to gradient,” *PLoS Biol.*, vol. 22, no. 6, 2024, Art. no. e3002669.
- [39] H. Li et al., “Atypical hierarchical connectivity revealed by stepwise functional connectivity in aging,” *Bioengineering*, vol. 10, no. 10, 2023, Art. no. 1166.
- [40] E. Koechlin, C. Ody, and F. Kouneiher, “The architecture of cognitive control in the human prefrontal cortex,” *Science*, vol. 302, no. 5648, pp. 1181–1185, 2003.
- [41] R. Cabeza, L. Nyberg, and D. C. Park, *Cognitive Neuroscience of Aging: Linking Cognitive and Cerebral Aging*. New York, NY, USA: Oxford Univ. Press, 2016.
- [42] M. N. Rajah and M. D’Esposito, “Region-specific changes in prefrontal function with age: A review of pet and fMRI studies on working and episodic memory,” *Brain*, vol. 128, no. 9, pp. 1964–1983, 2005.
- [43] D. T. Stuss and R. T. Knight, *Principles of Frontal Lobe Function*. New York, NY, USA: Oxford Univ. Press, USA, 2013.
- [44] O. Sporns, “The human connectome : A complex network,” *Ann. New York Acad. Sci.*, vol. 1224, pp. 109–125, 2011.
- [45] R. Ishii et al., “Healthy and pathological brain aging: From the perspective of oscillations, functional connectivity, and signal complexity,” *Neuropsychobiology*, vol. 75, no. 4, pp. 151–161, 2018.
- [46] L. Koelewijn et al., “Alzheimer’s disease disrupts alpha and beta-band resting-state oscillatory network connectivity,” *Clin. Neurophysiol.*, vol. 128, no. 11, pp. 2347–2357, 2017.
- [47] V. Gutiérrez-de Pablo et al., “Exploring the disruptions of the neurophysiological organization in Alzheimer’s disease: An integrative approach,” *Comput. Methods Programs Biomed.*, vol. 250, 2024, Art. no. 108197.
- [48] P. M. Rossini et al., “Neurophysiological hallmarks of neurodegenerative cognitive decline: The study of brain connectivity as a biomarker of early dementia,” *J. Personalized Med.*, vol. 10, no. 2, 2020, Art. no. 34.
- [49] M. S. Rafi and P. S. Aisen, “Detection and treatment of Alzheimer’s disease in its preclinical stage,” *Nature aging*, vol. 3, no. 5, pp. 520–531, 2023.